

Calculation of Ionization Energy, Electron Affinity, and Hydride Affinity Trends in Pincer-Ligated d^8 -Ir($t\text{Bu}^4\text{PXCXP}$) Complexes: Implications for the Thermodynamics of Oxidative H_2 Addition

Abdulkader Baroudi,^{†,||} Ahmad El-Hellani,[†] Ashfaq A. Bengali,[‡] Alan S. Goldman,[§] and Faraj Hasanayn^{*,†}

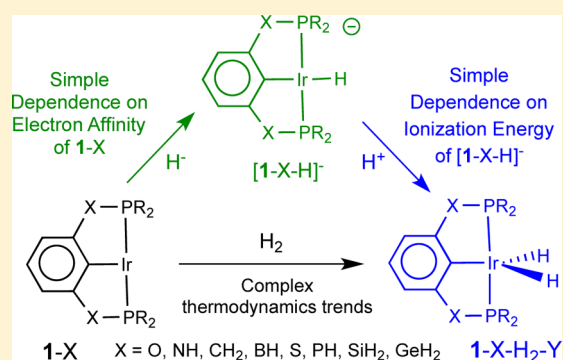
[†]Department of Chemistry, The American University of Beirut, Beirut, Lebanon

[‡]Department of Chemistry, Texas A&M University at Qatar, Doha, Qatar

[§]Department of Chemistry and Chemical Biology, Rutgers, The State University of New Jersey, New Brunswick, New Jersey 08903, United States

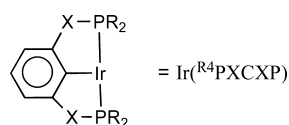
Supporting Information

ABSTRACT: DFT methods are used to calculate the ionization energy (IE) and electron affinity (EA) trends in a series of pincer ligated d^8 -Ir($t\text{Bu}^4\text{PXCXP}$) complexes (**1-X**), where C is a 2,6-disubstituted phenyl ring with X = O, NH, CH₂, BH, S, PH, SiH₂, and GeH₂. Both C_{2v} and C_2 geometries are considered. Two distinct σ -type (2A_1 or 2A) and π -type (2B_1 or 2B) electronic states are calculated for each of the free radical cation and anion. The results exhibit complex trends, but can be satisfactorily accounted for by invoking a combination of electronegativity and specific π -orbital effects. The calculations are also used to study the effects of varying X on the thermodynamics of oxidative H_2 addition to **1-X**. Two closed shell singlet states differentiated in the C_2 point group by the d^6 -electron configuration are investigated for the five-coordinate Ir(III) dihydride product. One electronic state has a d^6 - $(a)^2(b)^2(b)^2$ configuration and a square pyramidal geometry, the other a d^6 - $(a)^2(b)^2(a)^2$ configuration with a distorted-Y trigonal bipyramidal geometry. No simple correlations are found between the computed reaction energies of H_2 addition and either the IEs or EAs. To better understand the origin of the computed trends, the thermodynamics of H_2 addition are analyzed using a cycle of hydride and proton addition steps. The analysis highlights the importance of the electron and hydride affinities, which are not commonly used in rationalizing trends of oxidative addition reactions. Thus, different complexes such as **1-O** and **1-CH₂** can have very similar reaction energies for H_2 addition arising from opposing hydride and proton affinity effects. Additional calculations on methane C–H bond addition to **1-X** afford reaction and activation energy trends that correlate with the reaction energies of H_2 addition leading to the Y-product.



INTRODUCTION

The use of pincer ligands impacts many areas of modern transition metal chemistry.^{1,2} As tridentate chelates, pincer ligands offer several channels to tune the electronic and steric environments of unsaturated metal fragments of relevance to catalysis.³ The focus of the present study is a class of three-coordinate d^8 -Ir($R^4\text{PXCXP}$) fragments (**1-X**) implicated as C–H activating species in catalytic alkane dehydrogenation^{4,5} and uniquely suited for homogeneous tandem catalyzed alkane metathesis.⁶ The species used as a catalyst precursor in such reaction is typically an olefin complex or the five-coordinate iridium dihydride (Ir($R^4\text{PXCXP}$)(H)₂).^{4–8}



This class of catalysts has been the subject of extensive structure–activity studies that attempted to improve the activity

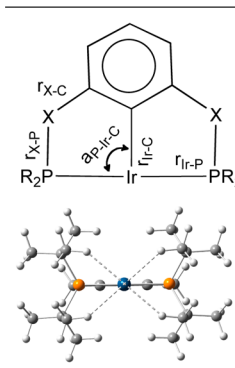
by varying the linker X, changing the phosphino group, or introducing varied substituents on the aromatic ring of the pincer ligand.^{4–9} The results afforded subtle effects on both catalytic activity and product distribution (in tandem metathesis).^{4–9}

The addition of a C–H bond to **1-X** is generally accepted to be the entry step to catalytic alkane dehydrogenation.^{10,11} Although it may not necessarily be the rate-limiting step in catalysis,⁸ the energetics of this step will always be critical to the activity and presumably to product distribution in alkane metathesis. C–H addition to a metal is generally classified as oxidative with respect to the metal; thus, simplistically, one would expect the reaction to be favored by metal centers that are more electron rich. DFT calculations on the reaction of alkanes with **1-X** indicated that the introduction of oxygen linkers (X) on the pincer ligand and alkoxy substituents on the

Received: July 3, 2014

Published: November 18, 2014



Table 1. Geometric Parameters of 1-X Optimized in C_{2v} (in Å and deg)


X	r_{X-C}	r_{Ir-P}	a_{P-Ir-C}	r_{Ir-P}	r_{Ir-C}	r_1
O	1.37	1.66	80	2.29	1.96	5.6
NH	1.40	1.69	82	2.29	1.98	5.4
CH ₂	1.50	1.84	85	2.30	1.97	5.0
BH	1.51	1.93	88	2.34	1.93	4.9
S	1.79	2.12	89	2.30	1.98	4.7
PH	1.78	2.10	94	2.32	2.01	4.5
SiH ₂	1.85	2.24	94	2.33	1.99	4.4
GeH ₂	1.94	2.30	95	2.33	2.01	4.4

aromatic group favor both the thermodynamics and kinetics of C–H addition.⁹ Given that oxygen is a strongly electronegative substituent, these findings were noted to be rather counter-intuitive, and were qualitatively attributed to the π -donating character of the oxygen atom. However, the detailed mechanism by which such π -effects would promote oxidative addition remained unclear.

The ionization energy (IE) and electron affinity (EA) of transition metal complexes and their matching redox potentials are fundamental entities that play a direct role in dictating the thermodynamics (and presumably the kinetics) of metal–ligand bond formation and dissociation. The redox potentials are of course also essential ingredients used in the design of molecular electrocatalysts.^{12,13} In addition, the IEs and EAs would offer quantifiable observables to gauge common qualitative notions such as the electron richness of metal center, which are often invoked in rationalizing thermodynamic trends, particularly for oxidative addition reactions. However, there have been limited experimental and theoretical investigations of the redox properties of pincer complexes,^{14,15} and to our knowledge, they have not been investigated in the three-coordinate Ir(^R4PXCXP) system.

In the present work we use electronic structure methods to calculate the IE and EA trends of a series of Ir(^R4PXCXP) (1-X) complexes where R is a t-butyl group and X is a systematically varied linker. The computed trends are found to be complex, but they can be satisfactorily explained by invoking a combination of electronegativity and specific π -orbital interaction effects. The calculations are then used to explore if the IE and EA trends can be helpful in understanding the thermodynamics of the oxidative addition of H₂ to 1-X. We chose to work with H₂ because the symmetry of the product allows clarification of important electronic (molecular orbital) aspects of the reaction, and because the thermodynamics of H₂ addition play a key role in determining the energetics of alkane dehydrogenation and related reactions catalyzed by such species. We find no simple correlations between the computed reaction energies of H₂ addition and either the IEs or EAs. However, we show that the IEs and EAs are valuable in rationalizing the thermodynamic trends when the H₂ addition reaction is broken into a sequence of hydride and proton addition components. Brief calculations on methane addition to 1-X indicate that the findings for the H₂ addition reaction apply to both the thermodynamics and kinetics of C–H addition.

COMPUTATIONAL METHODS

The calculations were carried out using Gaussian 09.¹⁶ Geometry optimization and normal mode vibrational analysis were done in the

gas phase at the M06 DFT level.¹⁷ The nonmetal elements carried the 6-311G++(2d,2p) basis set.¹⁸ For iridium, the 60 core electrons were replaced by the Hay–Watt relativistic effective core potential (ECP).¹⁹ The basis set on the valence electrons of iridium included the double- ζ functions supplied with the ECP, along with two polarization functions with exponents 0.94 and 0.3,²⁰ and one diffuse function with exponent 0.015.²¹ Additional electronic energies were obtained by single point calculations on the gas phase geometries in a polarizable continuum (PCM)²² representing THF as solvent. The trends in the gas phase and the PCM continuum are similar. We present the gas phase results in the text, and we give the PCM results as Supporting Information. Because the main focus of the present study is to understand the electronic effects of the substituents, we base the discussion on the electronic energies (E) rather than on enthalpies or free energies.

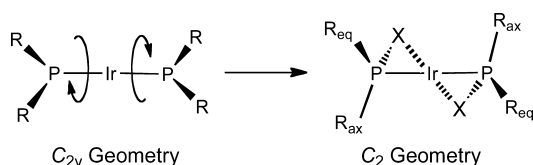
RESULTS AND DISCUSSION

Geometry Considerations. We consider the set of the eight linkers specified in Table 1. All of the complexes have a C_2 equilibrium geometry. However, for 1-O, 1-NH, and 1-S, the five-membered metallacycle ring is nearly planar, bringing the geometry close to C_{2v} . For X = CH₂, BH, S, PH, SiH₂, and GeH₂ on the other hand, the metallacycle rings are pronouncedly puckered. In order to evaluate if puckering is likely to play a role in the redox trends, we find it useful to include calculations in which the geometry of all of the complexes is optimized in the constraints of the C_{2v} point group.

Geometry of 1-X in C_{2v} . The complexes in Table 1 are listed in the order of increasing size of X. Thus, in going from 1-O to 1-GeH₂ the X–C bond distance (r_{X-C}) increases from 1.37 to 1.97 Å, and the X–P distance (r_{X-P}) increases from 1.66 to 2.30 Å. The lengthening of the pincer arm is accompanied by an increase in the P–Ir–C angle from 80° to 95°. As demonstrated in Table 1, the four equivalent t-butyl groups in 1-X create a “cavity” around the vacant coordination site trans to the phenyl carbon. The relative size of the cavity can be conveniently evaluated from the diagonal distance between the hydrogen atoms of the methyl groups (r_1 in Table 1). This distance decreases from 5.6 in 1-O to 4.4 Å in 1-Ge, thus suggesting the linkers can exert significantly different steric effects in the reactions of 1-X. Finally, 1-X exhibits pronounced variations in the bond distances involving the metal: r_{Ir-P} = 2.29–2.34 Å, and r_{Ir-C} = 1.93–2.01 Å.

Geometry of 1-X in C_2 . The C_2 geometry can be obtained from C_{2v} by rotation of the iridium-phosphine bonds in opposite direction while retaining the planarity of the IrCPP moiety (iridium and the coordinating atoms).

The rotation displaces the X linkers out of the IrCPP plane and differentiates the alkyl groups of each phosphine into axial

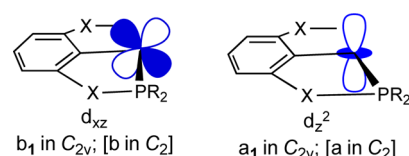


and equatorial sites. In C_2 the aromatic ring and the two X linkers remain largely (but not exactly) planar, so when the Ir–P bonds are rotated, the aromatic ring is twisted relative to the IrCPP plane. We use the dihedral angle d_1 defined in Table 2 to quantify the degree of puckering in the different complexes. For the linkers of the elements of the second period, d_1 increases in the following order: 0.5° (O) $\approx 2.6^\circ$ (NH) $< 12.6^\circ$ (CH_2) $< 24.8^\circ$ (BH). In 1-S the planarity of the metallacycle is recovered ($d_1 = 4.1^\circ$). For X = PH, SiH_2 , and GeH_2 , on the other hand, d_1 is large ($26\text{--}37^\circ$). The puckering does not cause much change in the P–Ir–C angle of the metallacycle ring ($a_{\text{P-Ir-C}} = 80\text{--}95^\circ$ in C_{2v} compared to $80\text{--}92^\circ$ in C_2), so the larger linkers continue to push the phosphines closer to the vacant coordination site. However, because the alkyl groups on each phosphine become inequivalent in C_2 , one of the diagonal distances between the inequivalent methyl groups in C_{2v} (r_1 , Table 1) is shortened, and the other is lengthened (r_{1a} vs r_{1b} in Table 2).

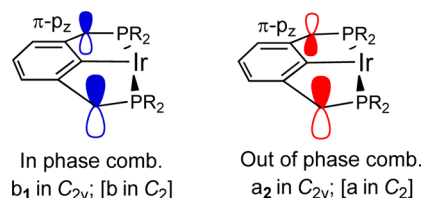
Table 2 includes the relaxation energy obtained when the constrained C_{2v} geometry is minimized into the equilibrium C_2 geometry (E_{relax}). As expected, for X = O, NH, or S for which the structural changes are minor, E_{relax} is small (0.6–1.2 kcal/mol). A relatively small relaxation energy is also computed for 1- CH_2 and 1-BH, 2.3 and 3.6 kcal/mol, respectively, even though the twist is not small, $d_1 = 12.6^\circ$ and 24.8° , respectively. For X = SiH_2 and GeH_2 , the geometry change is large, and E_{relax} is substantial (ca. 8.0 kcal/mol). Finally, for X = PH, E_{relax} is 58.2 kcal/mol; this follows from the high energy needed to invert the pyramidal geometry of alkyl phosphines, which typically have R–P–R angles close to 95° .

Ionization Energy of 1-X. In C_{2v} , 1-X will have a d^8 (a_2)²(b_2)²(b_1)²(a_1)² electron configuration, where a_1 is a d_{z^2} -type MO perpendicular to the molecular plane and b_1 is a π -type MO in a plane perpendicular to the molecular plane and containing the Ir–C bond (d_{xz} when the C_2 axis is defined as the x -axis). In C_2 the two valence MOs continue to have different symmetries (b or a).

Relevant to the discussion are the two equivalent π -type p_z AOs of the linker whose in-phase and out-of-phase



combinations transform as b_1 and a_2 , respectively, as shown below.



Actual displays of the valence filled MOs in 1-X for X = O, CH_2 , and BH in the C_2 geometries are shown in Scheme 1.

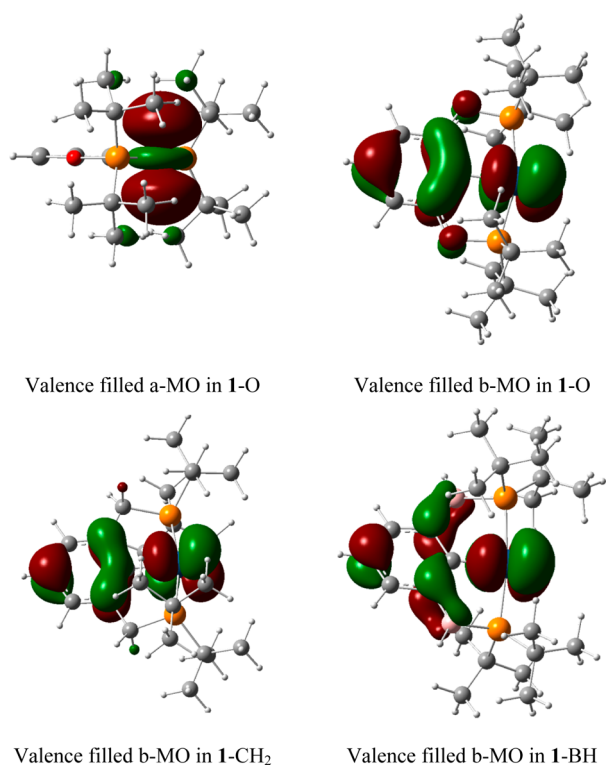
For all substituents, the filled valence a-MO in 1-X has nearly pure d_{z^2} character, as illustrated for 1-O in Scheme 1. In contrast, the valence filled b-MO is mixed with one of the filled π -MOs of the aromatic ring. When X = O, the b-MO acquires antibonding character due mixing with the filled b-combination of the two π -MOs on the oxygen linkers. When X = CH_2 , the contribution from the linker to the valence b-MO is largely reduced. When X = BH, on the other hand, the b-combination of the π -MOs from the linkers are empty, and they mix in an in-phase mode with the filled b-MO (Scheme 1).

In conducting the present study, we investigated the two vertical IEs corresponding to removal of an electron from either the valence d_{z^2} or the d_{xz} orbitals, thus leading, respectively, to 2A_1 and 2B_1 states of the free radical cations in C_{2v} , or to 2A and 2B states in C_2 . In the gas phase the 2A_1 IE of 1-O is predicted to be slightly greater than the 2B_1 IE: 145.7 vs 142.4 kcal/mol. Including a polarizable continuum representing THF as solvent in the calculation via the PCM model lowers the two IEs to 109.5 and 108.8 kcal/mol, respectively. With the SMD solvent continuum model²³ the IEs are lowered further and the 2A_1 state of the cation becomes slightly stabilized over 2B_1 (97.3 vs 98.8 kcal/mol). Although the absolute IEs from these calculations vary considerably, the results are in agreement that the energies of the 2A_1 and 2B_1 states in the ionized 1-O are close. The overall effects of the solvent apply systematically through the series, so the trends in the gas and solvent-continuum phases are comparable. The gas phase IEs obtained

Table 2. Geometric Parameters of 1-X Optimized in C_2 (in Å and deg)

X	d_1	$a_{\text{P-Ir-C}}$	$r_{\text{I-P}}$	r_1 (a)		E_{relax} (b)
				r_{1a}	r_{1b}	
O	0.5	80	2.29	5.5	5.9	0.6
NH	2.6	83	2.29	5.4	5.7	1.2
CH_2	12.6	84	2.30	5.2	5.9	2.3
BH	24.8	86	2.32	3.8	7.1	3.6
S	4.1	89	2.29	4.7	4.9	0.9
PH	26.4	88	2.31	4.9	6.3	58.2
SiH_2	32.4	91	2.32	3.8	6.6	7.7
GeH_2	35.9	92	2.32	3.5	6.7	8.1

^a r_{1a} and r_{1b} are the shortest distances between hydrogens of equivalent front phosphino-methyl groups. ^b E_{relax} is the energy difference between the C_{2v} and C_2 geometries in kcal/mol.

Scheme 1. Display of the Valence a and b MOs in 1-X (C_2 Geometry)

in C_{2v} and C_2 are given in Table 3, and the trends are displayed in column formats in Figure 1.

For the complexes with the linkers of the second period elements the 2A_1 IEs (blue columns) follow the trend 145.7 (O) > 137.4 (NH) \approx 136.0 (CH₂) < 141.2 (BH) (kcal/mol). For this set different trends are computed for the 2B_1 state (red columns), namely, 142.4 (O) \gg 131.5 (NH) < 135.3 (CH₂) \ll 146.2 (BH). In interpreting these trends we propose a qualitative model based on interplay between inductive electronegativity effects and specific π -MO interaction ones. Obviously, an increased electronegativity of the substituents on the ligands of a given complex is expected to decrease the electron density on the metal center and thereby cause an increase in the IE. However, in 1-X the variable substituents are part of the two five-membered rings that include the metal, so their π -properties can be transmitted to the metal through specific MO interactions with the aromatic ring as well as the phosphine ligands, and this can lead to distinct π -effects on the

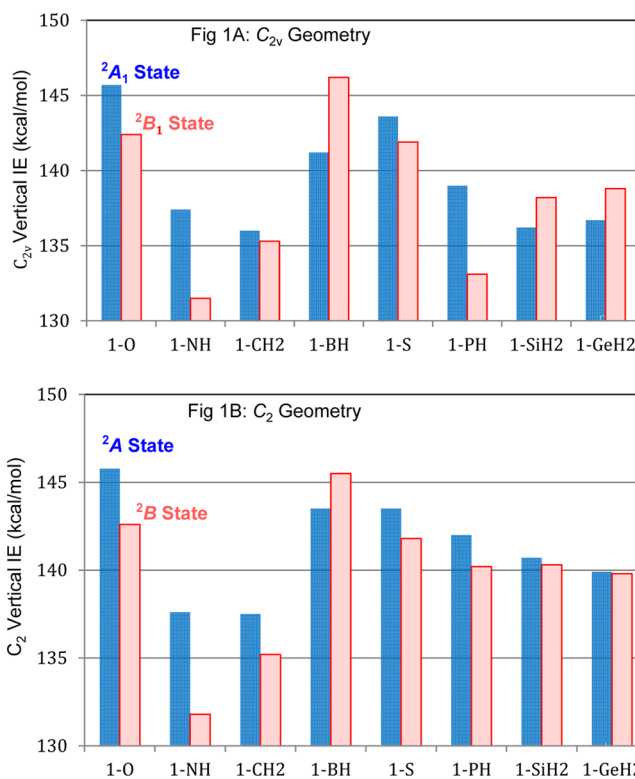
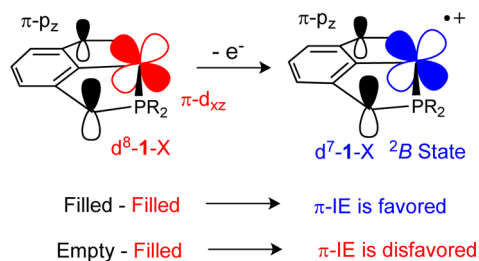


Figure 1. Vertical ionization energy of 1-X in the C_{2v} and C_2 geometries.

IEs. When X has a filled π -MO (such as X = O, NH, and S), it will destabilize the metal based π -MOs, such as d_{xz} and make it easier to ionize 1-X. Conversely, when the π -MOs on the linkers are empty (as in 1-BH and to some extent in 1-SiH₂), the metal π -orbitals will be stabilized, so the IEs are expected to become larger.



Compared to the oxygen atom, the NH group is less electronegative, so this should contribute to a smaller IE in 1-

Table 3. Vertical IEs of 1-X (in kcal/mol) and NBO Charges

X	C_{2v} geometry (Figure 1A)			C_2 geometry (Figure 1B)				
	2A_1	2B_1	gap	2A	2B	gap	δ_{Ir}^a	δ_P^a
O	145.7	142.4	3.3	145.8	142.6	3.2	-0.52	1.48
NH	137.4	131.5	5.9	137.6	131.8	5.8	-0.52	1.37
CH ₂	136.0	135.3	0.7	137.5	135.3	2.2	-0.50	1.16
BH	141.2	146.2	-5.0	143.0	145.5	-2.5	-0.39	0.78
S	143.6	141.9	1.7	143.5	141.8	1.7	-0.51	1.00
PH	139.0	133.1	5.9	142.0	140.2	1.8	-0.50	0.81
SiH ₂	136.2	138.2	-2.0	140.7	140.3	0.4	-0.49	0.66
GeH ₂	136.7	138.8	-2.1	139.9	139.8	0.1	-0.49	0.69

$^a\delta_{Ir}$ and δ_P are the NBO charges on the iridium and the phosphorus atoms, respectively, in atomic charge units.

NH. At the same time the planarized NH is a stronger π -donor than the oxygen, and this should also favor the ionization of 1-NH. The combined electronegativity and π -effects can therefore account for the large drop in the 2A_1 IE in going from 1-O to 2-NH. Upon substitution of NH by CH_2 both the electronegativity and the π -donating ability of X are reduced. The two factors should have opposite effects on the IEs, so this can explain the relatively small difference between the IEs of 1-NH and 1- CH_2 . In support of a role for distinct π -effects in the given two substitutions, the 2B_1 - 2A_1 gap is increased from 3.3 kcal/mol in the ionized 1-O to 5.9 in 1-NH, and is then lost in the free radical cation of 1- CH_2 (0.7 kcal/mol).

Substitution of CH_2 by the BH group continues to lower the electronegativity of X, but it now introduces a strong π -accepting character to the linker. According to the above discussion, the two factors should have opposite effects on the IE. The calculations predict both the 2A_1 and 2B_1 IEs of 1-BH to be much smaller than those of 1- CH_2 , suggesting the effects of the empty π -MOs on the two boron centers offset the electronegativity effects. Consistently, the order of the 2A_1 and 2B_1 states is reversed in the cation of 1-BH, with 2B_1 becoming a full 5.0 kcal/mol higher than 2A_1 (141.2 vs 146.2 kcal/mol). Note that in 1-BH the distance between iridium and the aromatic-ring (r_{Ir-C} , Table 1) is 1.93 Å, significantly shorter than r_{Ir-C} in 1- CH_2 (1.98 Å). This undoubtedly reflects an increased backbonding from the metal to the boron-substituted phenyl ring in 1-BH. In contrast, the Ir-P bond distances in 1-BH are significantly longer than those in 1- CH_2 (2.34 vs 2.30 Å). Presumably there is also some π -donation from the phosphines to the empty boron orbitals that reduces electron donation from the phosphines to the metal. Such effects can be relevant to the large increase in the 2A_1 IE when CH_2 is substituted by BH. In other words, the proposed inductive and π -effects appear to apply synergistically rather than independently.

Changing the oxygen linker in 1-X into sulfur is predicted to have only minor effects on the 2A_1 and 2B_1 IEs, lowering them by 2.1 and 0.5 kcal/mol, respectively. This is probably due to effects from decreased electronegativity (favoring ionization) and decreased π -donation (disfavoring ionization) in the sulfur linker.

Substitution of sulfur by the planarized PH linker in 1-X lowers the IEs of the 2A_1 and 2B_1 states by 4.4 and 8.8 kcal/mol, respectively, thereby increasing the 2A_1 - 2B_1 gap to 5.9 kcal/mol. These effects are similar to the ones calculated when oxygen is substituted by NH, so they too suggest a role for π -donation from the planar PH unit. The SiH_2 linker would be less electronegative than PH, but it should have some π -accepting character. Consistent with our qualitative propositions, substitution of PH by SiH_2 in 1-X decreases the 2A_1 IE but increases the 2B_1 IE. Thus, as found for 1-BH, the 2A_1 state becomes the ground state in the ionized 1- SiH_2 . Finally, the IEs of 1- SiH_2 and 1- GeH_2 are comparable.

The vertical ionization energies computed using the equilibrium C_2 geometries of 1-X are plotted in Figure 1B. For the series from 1-O to 1-BH the trends in the 2A and 2B IEs are qualitatively similar to the matching ones in C_{2v} . This is not unexpected since the two geometries are not very different in this series. In contrast, for 1-S, 1-PH, 1- SiH_2 , and 1- GeH_2 series the large variations computed in C_{2v} are lost in C_2 . For the latter complexes the 2A and 2B states are nearly degenerate in C_2 and the complete set of IEs vary within 3 kcal/mol. This indicates that pyramidalization of the PH linker in C_2 and the

increased puckering in 1-PH and 1- SiH_2 reduce (but not necessarily eliminate) the π -effects of the PH and SiH_2 linkers on the IE.

Table 3 includes the NBO charges computed on the metal (δ_{Ir}) and the phosphorus atoms (δ_P) of 1-X (C_2 geometry). Except for 1-BH where δ_{Ir} is -0.39 , the charge on the metal on all of the other complexes is nearly constant at -0.5 atomic charge units. In contrast, δ_P is positive and exhibits substantial variations consistent with expectations based on the electronegativity of the linker. Clearly, the computed IE trends cannot be explained in terms of either set of charges.

Finally the geometries of the free radical cations of 1-X were optimized in the C_2 point group in the gas phase.^{24,25} The relaxed IEs obtained using these geometries are only slightly smaller than the vertical IEs, but the trends in the two sets remain to be overall similar.

Electron Affinity of 1-X. 1-X has one vacant metal-based d-type MO along the empty coordination site (with antibonding character) and another one perpendicular to the molecular plane (the p_z AO). As before, the different symmetry of the two orbitals, a and b, respectively, allows the calculation of distinct electronic states of the free radical anion. The electron affinities (EAs) leading to the two states are given in Table 4, and the trends are displayed in Figure 2.

Table 4. Vertical Electron Affinity (EA) of 1-X (in kcal/mol)

X	C_{2v} geometry (Figure 2A)		C_2 geometry (Figure 2B)	
	2A_1	2B_1	2A	2B
O	17.8	-10.9	17.9	-10.2
NH	11.2	-13.9	11.2	-12.2
CH_2	7.7	-13.1	8.7	-11.4
BH	9.9	10.7	NA	8.4
S	21.9	-8.5	22.0	-8.2
PH	24.6	-14.3	14.4	-7.8
SiH_2	14.9	-9.7	11.3	-12.5
GeH_2	17.4	-10.3	11.7	-11.8

For the 2A_1 state EA decreases uniformly in going from 1-O (17.8), to 1-NH (11.2), to 1- CH_2 (7.7 kcal/mol). The same trend is computed for the corresponding 2A state in C_2 (both compared in Figure 2A using dark and light blue columns, respectively). This trend can be attributed straightforwardly to the accompanying decrease in the electronegativity of the linkers which should disfavor electron addition to 1-X. For 1-BH, the 2A_1 EA is increased slightly relative to 1- CH_2 . As discussed above, the strong π -accepting character of BH can delocalize the electron density away from the metal, and the effect can be transmitted to the a_1 MO. When the C_2 geometry of 1-BH is considered, the unpaired electron in the 2A state occupies the π -MO resulting from the out of phase combination of the p_z -orbitals of the two boron centers affording an EA value of 19.2 kcal/mol. This state corresponds to the π - 2A_2 state in C_{2v} , so it is not included in the table or the figure.

Substitution of the oxygen linker by sulfur increases the 2A_1 EA by 4.5 kcal/mol. This is a large effect that cannot be explained on the basis of the electronegativity differences of the two substituents. Substitution of sulfur by PH in C_{2v} increases the 2A_1 EA further to 24.6 kcal/mol, which appears to be anomalously large. However, for the C_2 geometry, the 2A EA of 1-PH is lowered to 14.6 kcal/mol. For 1- SiH_2 the 2A_1 and 2A EAs are 14.9 and 11.3 kcal/mol, respectively. Thus, in C_2 the 2A

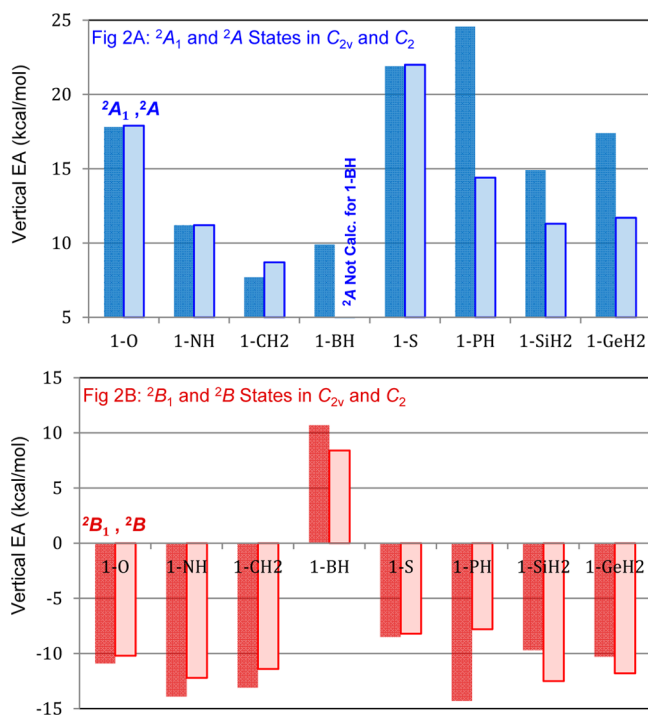


Figure 2. Vertical electron affinity of 1-X in the C_{2v} and C_2 geometries.

EAs of 1-S, 1-PH, and 1-SiH₂ follow the same (decreasing) order as in the 1-O, 1-NH, and 1-CH₂ series, and can therefore be attributed in a simple way to the electronegativity which decreases in the order $S > PH > SiH_2$.

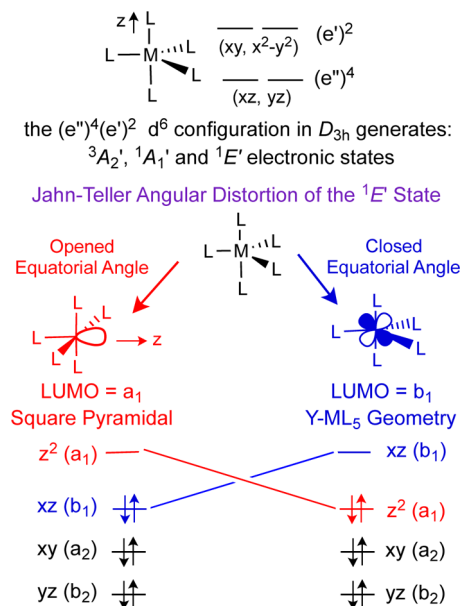
The vertical EAs leading to the 2B_1 (C_{2v}) or 2B (C_2) states are compared in Figure 2B. Except for 1-BH, these EAs are all negative (disfavored). For 1-BH on the other hand the unpaired electron is delocalized over the boron $2p_z$ -AOs, and the EA is positive. When 1-BH is excluded from the analysis, the 2B EAs in C_2 exhibit relatively small variations. Given the unfavorable energy of this state we do not attempt to analyze the corresponding trends.

H₂ Addition to 1-X: Jahn–Teller Effects. In the remaining parts of the study we consider the oxidative H₂ and methane C–H bond addition reactions of 1-X, and we explore if the above IE and EA trends can be useful in rationalizing the computed thermodynamics trends. The discussion will focus on H₂ addition where the applicable C_2 symmetry can be utilized to distinguish between different electronic states in the d^6 five-coordinate products.

H₂ addition to 1-X affords an electronically and coordinatively unsaturated d^6 -Ir(III) dihydride product. The problem of the geometry and electronic structure in this system has been the subject of previous theoretical investigations.^{26,27} Briefly, in an idealized D_{3h} trigonal bipyramidal geometry a d^6 -ML₅ complex will have a d^6 (e'')⁴(e')² electron configuration (Scheme 2). This configuration generates one triplet state (${}^3A_2'$), one open shell singlet state (${}^1A_1'$), and one closed shell state (${}^1E'$). The ${}^1E'$ state is electronically degenerate, so it will be subject to the Jahn–Teller effect.²⁸

One accessible angular distortion mode that can lift the ${}^1E_1'$ degeneracy pertains to opening or closing one of the equatorial angles of the D_{3h} geometry. Opening the angle places two of the equatorial ligands in a T-arrangement thus affording a square pyramidal geometry. Closing the equatorial angle leads to a distorted trigonal bipyramidal structure in which the

Scheme 2. MO-Occupancies Differentiating the Electronic States with Square Pyramidal and Y Geometries of d^6 -ML₅ Complexes



equatorial ligands are in a Y-arrangement (Scheme 2). The two geometries correspond to different closed shell electronic states differentiated by the d^6 -orbital occupancies. As illustrated in Scheme 2, the HOMO and LUMO in the T-geometry have b_1 (π) and a_1 (σ) symmetries. In the Y-geometry, the occupancy of these orbitals is switched. When the ligands are equivalent, one geometry will be a minimum, the other a transition state connecting two equivalent minima in a Mexican hat type potential energy surface. Related angular Y and T distortion modes are known for the closed shell state of unsaturated 16-electron piano stool complexes.^{29,30} When the three equatorial ligands are different (heteroligands), the order of the Y and T states can be altered depending on the nature of the substituents.²⁹

Experimentally, the distorted trigonal bipyramidal Y-geometry is ubiquitous among the isolable d^6 ruthenium, rhodium, and iridium phosphino hydride complexes having one π -donor ligand, such as an alkoxide,^{31,32} a halogen,³³ or an amide.³⁴ The unusual stability of these coordinatively and electronically unsaturated complexes is commonly attributed to the availability of the empty π -type MO on the metal in the Y geometry ($b_1 = d_{xz}$ in Scheme 2), which stabilizes the complexes by imparting a double bond character to the metal–ligand bond, which would satisfy an 18-electron configuration on the metal.

In studying H₂ addition to 1-X we calculated both the symmetrical Y and the symmetrical T geometries, 1-X-H₂-Y and 1-X-H₂-T in eq 1. The reaction energies for the transformation from the separated reactants to each product are given in Table 5 (ΔE_Y and ΔE_T , in kcal/mol).

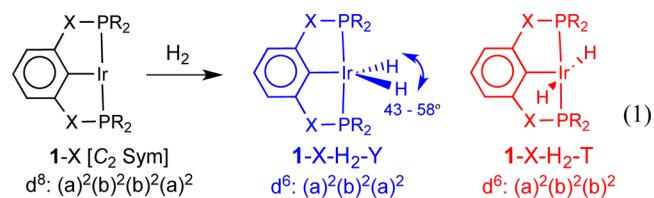


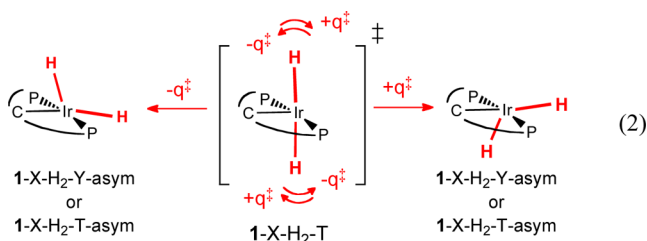
Table 5. Reaction Energies for H₂ Addition to 1-X (in kcal/mol)^a

X	1-X-H ₂ -Y			1-X-H ₂ -T			
	ΔE _Y	ΔG ^o _Y	HlrH	ΔE _T	ΔG ^o _T	ν [‡] _T (cm ⁻¹)	ΔE _{Y,T}
O	-29.6	-19.4	57°	-8.2	2.9	29Si	21.5
NH	-30.4	-20.4	58°	-10.3	2.6	206i	20.0
CH ₂	-27.6	-16.6	50°	-13.7	-0.9	117i	13.9
BH	-22.1	-12.8	43°	-9.6	1.3	51i	12.5
S	-29.4	-16.5	58°	-10.2	4.7	207i	19.3
PH	-25.8	-15.9	53°	-12.7	-0.9	52i	13.1
SiH ₂	-24.6	-13.3	56°	-12.9	-1.1	none	11.7
GeH ₂	-25.6	-13.7	56°	-12.8	-0.6	none	12.8

^aΔG^o is computed at 298 K and 1 atm.

For all substituents, the calculations predict the ground state to have the Y-geometry. For the complexes with the π-donor linkers (X = O, NH, and S) the Y-T gap is computed to be quite large: 19.3–21.5 kcal/mol. For the other substituents the gap is smaller, 11.7–13.9 kcal/mol. Thus, although the linker is not directly connected to the metal, the results are in line with the generally accepted view that π-donor ligands tend to stabilize the Y-state of unsaturated d⁶-ML₅ complexes.^{26,29,31}

The symmetrical Y and T geometries in eq 1 were computed in the constraints of the C₂ point group. Normal mode analysis confirms the Y geometry to be a true minimum on the PES for all substituents. For X = SiH₂ and GeH₂ the symmetrical T geometry is also a true minimum. For all the other complexes, on the other hand, the symmetrical T geometry has one vibration with an imaginary frequency (ν[‡] = 51i–295i cm⁻¹; Table 5). The coordinates of the imaginary frequency (q[‡]) are for motion of the two hydrides in a direction connecting two equivalent asymmetrical geometries (Y-asym, or T-asym) as illustrated in eq 2.

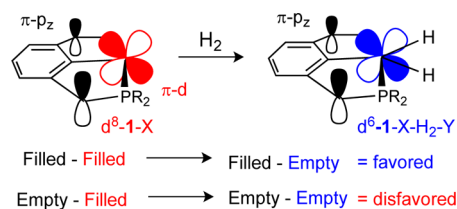


Because the asymmetric Y and T geometries are not very different, full geometry optimization in C₁ can identify only the lower energy geometry of the two stated. Thus, full geometry optimizations in the asymmetrical region of the PES converge to the asymmetrical Y-geometry when X = O, NH, CH₂, BH, and PH₂, and to the asymmetrical T-geometry when X = S, SiH₂, and GeH₂. These results reflect subtle dependencies of PESs on the linker X. For all substituents, the asymmetrical minimum (Y or T) is found to be significantly higher in energy than the symmetrical Y-geometry so we do not discuss the asymmetric geometry any further.

H₂ Addition: Thermodynamic Trends. In discussing the thermodynamics of H₂ addition to 1-X we find it useful to start with the trends in ΔE_T. We focus on the reactions of 1-O and 1-CH₂ because they have been already used for alkane dehydrogenation and showed comparable activity. For X = O, NH, and CH₂, the exothermicity increases gradually down the series ΔE_T = -8.2, -10.3, and -13.7 kcal/mol, respectively. This trend is consistent with the notion that complexes having

metal centers that are more electron rich (in this case due to decreased electronegativity of the linkers) would favor the thermodynamics of oxidative addition. Note however that the given ΔE_T trends do not follow the same ²A IE trends of 1-X, where the IEs of 1-NH and 1-CH₂ are similar (Figure 1A). Substitution of CH₂ by BH disfavors ΔE_T by 4.1 kcal/mol. Although this precludes making a general statement about the electronegativity effect, the result can still be attributed to decreased electron richness on the metal in 1-BH due to an exceptionally large π-accepting character of BH.

In contrast with the large and regular variations in ΔE_T, the differences in ΔE_Y in the 1-O, 1-NH, and 1-CH₂ series are computed to be small and irregular. Thus, changing 1-O to 1-NH changes the exothermicity by less than a kcal/mol. More importantly, and opposite to the order found for ΔE_T, ΔE_Y for 1-CH₂ is predicted to be less exothermic than for 1-O, -29.6 and -27.6 kcal/mol, respectively. As was the case with the ²A and ²B IEs, the different ΔE_T and ΔE_Y trends suggest a role for specific π-MO effects that oppose the electronegativity effect. The presence of filled π-AOs on the linkers in 1-X imparts a degree of antibonding character to the filled d_{xz} orbital of the metal (Scheme 1). When the Y-product is formed, the d_{xz} orbital (corresponding to the b₁-MO in Scheme 2) is emptied, so the antibonding interaction with the filled π-MOs of X is switched into a bonding one.



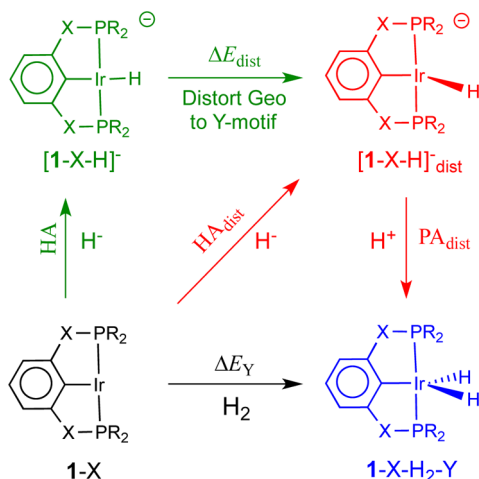
Such effects can explain why H₂ addition to 1-O (with two π-donor linkers) is more exothermic than addition to the presumably overall more electron rich 1-CH₂. In accord with this qualitative MO analysis, in the full series of complexes in Table 5, H₂ addition is least favored in 1-BH (ΔE_Y = -22.1 kcal/mol). In this case the linker has two empty p_z orbitals, so the π-interactions involving the filled d_{xz} will have a bonding character in the reactant that will be lost when d_{xz} is emptied in the Y-dihydride product. Note that when X = BH, the angle between the two hydrides is 43°, much smaller than any other complex (50–58°; eq 1 and Table 5). The H–H bond distance in the BH complex is 1.19 Å; thus, this species is close to a dihydrogen adduct.

Substitution of the oxygen linker by sulfur has relatively small effects on both ΔE_Y and ΔE_T. This finding is in line with the comparable IEs and EAs of 1-O and 1-S, as well as the comparable Y-T gap of the dihydride products. Substitution of sulfur by PH disfavors ΔE_Y by 3.6 kcal/mol (suggesting reduced π-stabilization in 1-PH-H₂-Y), but favors ΔE_T by 2.5 kcal/mol (which can be consistent with an effect due to decreased electronegativity). Finally, the exothermicities of H₂ addition to 1-PH, 1-SiH₂, and 1-GeH₂ are computed to be comparable (ΔE_Y ≈ -25 and ΔE_T ≈ -13 kcal/mol).

H₂ Addition in a Hydride–Proton Addition Cycle. The trends in ΔE_Y in Table 5 did not correlate in a simple way with the IE or EA trends in Tables 3 and 4. In the above section we attributed the ΔE_Y trends qualitatively to interplay between electronegativity and π-effects that can work in opposite ways. In an attempt to gain further insight into the origin of the variations (or similarities) in ΔE_Y, we break H₂ addition to 1-X

into a sequence of (i) hydride addition to 1-X, (ii) distortion of the iridium hydride intermediate, and (iii) protonation of the distorted iridium hydride into the final 1-X-H₂-Y product as illustrated in Scheme 3.

Scheme 3. H₂ Addition to 1-X via Hydride and Proton Addition Steps



Although we are not aware of prior studies that adopt such a cycle in making M(H)₂ products, heterolytic cleavage of H₂ into a hydride and a proton over (bifunctional) metal–ligand moieties, such as in Fryzuk’s iridium–amide complexes,^{31a} is well-known. Noyori proposed a role for bifunctional heterolytic H₂ cleavage in catalytic ketone hydrogenation by ruthenium amide complexes.³⁵ More recently, DuBois, Bullock, and co-workers designed novel electrocatalysts for H₂ oxidation/production based on complexes in which the metal adds a hydride from H₂ and a pendant neutral amine group acts as a base that captures the proton from H₂ (proton relay).^{36,37} The cycle in Scheme 3 simply corresponds to a heterolytic H₂ addition process in which the metal center is both the hydride acceptor and the proton acceptor. The factors that determine the ability of metal complexes to donate/accept a hydride (the hydricity, which is related to the hydride affinity of the metal) have been the subject of extensive experimental³⁸ and theoretical^{39,40} investigations. Likewise, the ability of metal complexes to give/accept a proton (metal hydride acidity or metal proton affinity) is important to many catalysts and applications and has accordingly been extensively studied both experimentally and computationally.^{41,42} The identity of the metal, the nature of the ligands, and the details of the geometry have been shown to play an important role in both the hydricity and acidity of metal complexes. In the H₂ addition reaction of 1-X, the metal is constant, and the geometrical changes (involving the coordination of the PXCXP ligand) are minor. Thus, variations of the energies of the hydride and proton addition steps are expected to be determined in large by electronic effects exerted by X. In elucidating these effects, we continue to work with gas phase electronic energies. The data are given in Table 6.

The hydride adds to the vacant σ -type metal orbital of 1-X to give a square planar product ([1-X-H][−]), so there is no change in the electronic state of in this step. For the set of O, NH, and CH₂ linkers, the hydride affinity (HA) decreases in the order 92.0 > 85.6 > 82.7 kcal/mol. This trend is similar to the electron affinity trend where the electron is also added to the

Table 6. Data for H₂ Addition to 1-X via Hydride and Proton Addition Steps as Defined in Scheme 3 (in kcal/mol)

X	hydride affinity of 1-X (Figure 3)			PA and IE of distorted [1-X-H] [−] (Figure 4)		undistorted [1-X-H] [−]	
	HA	ΔE_{dist}	HA _{dist}	PA _{dist}	IE _{dist}	IE (² B)	PA (Y)
O	92.0	9.2	82.8	353.5	37.6	53.7	344.3
NH	85.6	9.9	75.8	361.3	29.1	44.9	351.4
CH ₂	82.7	8.1	74.6	359.7	31.4	45.9	351.7
BH	82.1	5.4	76.7	351.6	46.8	55.6	346.2
S	94.4	9.3	85.1	351.0	39.3	54.3	341.7
PH	88.1	9.0	79.1	353.4	37.3	52.5	344.3
SiH ₂	85.7	10.5	75.2	356.1	34.4	51.5	345.6
GeH ₂	87.2	10.8	76.4	355.9	34.6	53.6	345.1

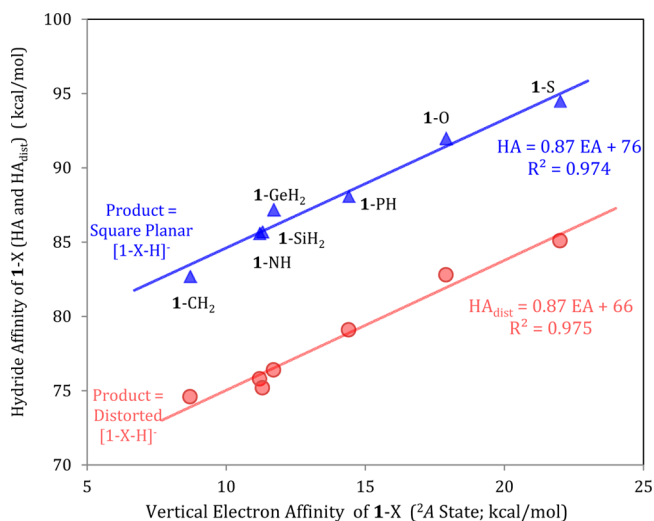


Figure 3. Hydride affinity vs electron affinity of 1-X.

empty σ -MO of 1-X (Table 4 and Figure 2A). Figure 3 shows the correlation between increased electron affinity and increased hydride affinity to extend through the full series of complexes. Thus, the complexes with the more electronegative substituents favor addition of a hydride. Note that 1-BH is excluded from Figure 3 because we were unable to calculate the ²A state of the free radical anion of 1-BH as discussed before.

To proceed with the cycle in Scheme 3, the square planar [1-X-H][−] is first distorted into [1-X-H][−]_{dist} corresponding to the structural motif of this moiety in the final 1-X-H₂-Y product. The distortion energies (ΔE_{dist}) among the different complexes are not very different ranging from 8.1 to 10.8 kcal/mol (Table 6). Accordingly, when the distorted hydride geometries are used to define the hydride affinity of 1-X (HA_{dist}; Scheme 3), the resulting trends continue to correlate satisfactorily with the electron affinities of 1-X (Figure 3).

Starting from the distorted [1-X-H][−]_{dist}, the computed proton affinity trends leading to 1-X-H₂-Y (PA_{dist}; Table 6) are more complex than the initial hydride affinity trends. For example, PA_{dist} increases from 353.5 to 361.3 kcal/mol when X = O is substituted by NH, but then decreases to 359.7 kcal/mol for X = CH₂. Nevertheless, Figure 4 shows PA_{dist} to correlate linearly with the vertical ionization energy of [1-X-H][−]_{dist} (IE_{dist}); thus, the proton affinity is apparently dominated by the oxidative component of protonation. Note that the calculated PA for [1-BH-H][−]_{dist} is 46.8 kcal/mol, much larger than in the other complexes. This result seems to follow from

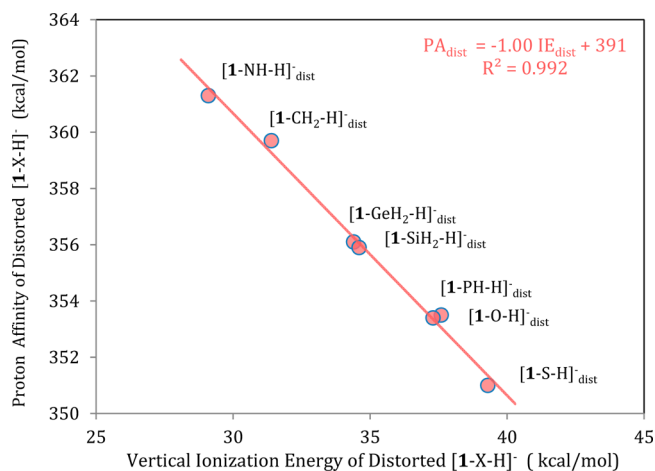


Figure 4. Proton affinity vs IE of the undistorted square planar $[1-X-H]^-$.

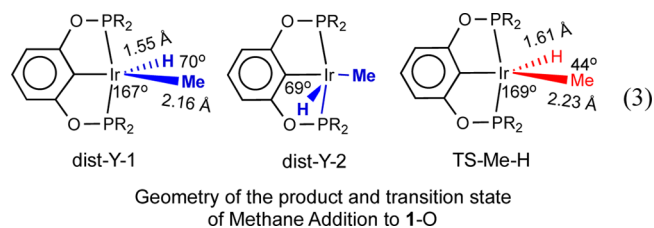
the fact that the distortion in this species is minor because $1-BH-H_2-Y$ is nearly a dihydrogen complex with $HIrH$ angle of 43° (Table 5).⁴³ Accordingly, we treat $1-BH$ as an outlier, and we exclude it from the analysis.

Interestingly, the calculated correlations in Figures 3 and 4 are in line with results from an experimental study that revealed the existence of free-energy relationships between the hydride and proton donor abilities of $[HNi(diphosphine)_2]^+$ complexes and the redox potentials of their conjugate bases.⁴⁴ Also significant, a recent analysis of an elaborate set of data on nickel electrocatalysts with pendant amines concluded that knowledge of only the I/O potential of the metal (which relates to EA) and the acidity of the amine suffices to predict a large number of thermodynamic parameters like the hydricity, and ultimately the energy of heterolytic H_2 addition/production.⁴⁵

To sum up, when $1-BH$ is excluded from the analysis, the ΔE_Y values for H_2 addition to $1-X$ vary within 6 kcal/mol (Table 5). The trends do not correlate with either the IEs or EAs of $1-X$, so we analyze them in Scheme 3 using a thermodynamic cycle of hydride and proton addition steps. Figure 3 shows there is a linear correlation between the hydride and electron affinities of $1-X$, and Figure 4 shows that the subsequent protonation step is linearly dependent on the IE of the intermediate iridium hydride ($[1-X-H]^-$). One would generally expect substituents that favor the EAs to disfavor the IEs. However, in the reaction leading to the Y dihydride product the hydride is added to an empty σ -type MO, whereas the proton is added to a filled π -type MO and involves distortion of the square planar geometry.⁴⁶ As such there is no reason to expect the two factors to cancel out or to expect one factor to systematically dominate the other. The computed variations in ΔE_Y reflect the different weights of the hydride and proton affinity components. The proposition in the previous section that the π -donor character of the oxygen linker plays a role in favoring H_2 addition to $1-O$ pertains to a specific MO effect which favors the protonation component of the reaction compared to an expectation based on the high electronegativity of oxygen alone. The proposed specific π -effect applies by making it easier to ionize the metal d_{xz} orbital.⁴⁶ However, Table 6 shows that $[1-O-H]^-$ still has one of the highest IEs in the series, so were it not for the very high hydride affinity, $1-O$ would not have such a highly favorable ΔE_Y .

Methane Addition. As mentioned in the Introduction, the three-coordinate fragment under consideration is generally proposed to be the active species in the activation of a C–H bond in the context of alkane dehydrogenation by $1-X$.^{10,11} Given that alkane addition to $1-X$ would also be classified as an oxidative addition step, it is of interest to examine if it shows a similar dependence on X as H_2 addition. In this section we address this question briefly for the reaction of methane.

Methane addition to $1-X$ affords a five-coordinate methyl hydride product with a distorted trigonal bipyramidal geometry. For $X = O$ two isomers with similar energy could be identified as true minima on the PES differentiated by whether the Ir–H bond makes an angle of ca. 70° with the methyl group (dist-Y-1) or with the bound carbon of the aromatic ring of the pincer ligand (dist-Y-2) as shown in eq 3.



For the purpose of a systematic comparison with the H_2 addition reaction leading to the symmetrical Y -dihydride product we consider only the dist-Y-1 isomer. However, for $X = CH_2$ and BH , geometry optimization always converges to dist-Y-2. To circumvent this problem we optimized the geometry of the latter two species with the $H-Ir-Me$ angle fixed at 70° . The geometries obtained this way do not exhibit any imaginary frequency. The relevant reaction energies are given in Table 7.

Table 7. Reaction and Activation Energies of Methane Addition to $1-X$ (in kcal/mol)^a

X	ΔE_{MeH}	ΔG°_{MeH}	ΔE^\ddagger_{MeH}	ΔG^\ddagger_{MeH}	ν^\ddagger_{TS} (cm ⁻¹)
O	-7.3	1.9	-4.2	4.6	609i
NH	-7.3	2.7	-3.5	5.6	606i
CH ₂	-2.3	7.9	0.3	10.5	600i
BH	2.0	11.7	5.7	14.5	627i
S	-3.8	8.3	0.6	13.0	615i
PH	1.5	11.0	3.8	13.8	560i
SiH ₂	3.7	16.4	6.4	18.5	552i
GeH ₂	3.7	14.8	6.6	18.4	559i

^aReaction leading to dist-Y-1 described in eq 3. G° computed at 298 K and 1 atm.

The energies of methane addition to $1-X$ are computed to exhibit a greater dependence on X than those for H_2 addition: $\Delta E_{MeH} = -7.3 + 3.7$ kcal/mol, compared to $\Delta E_{H_2} = -30.4 - 24.6$ kcal/mol ($1-BH$ is excluded from the comparison). Nevertheless, a plot of the two sets of energies reveals overall parallel trends (Figure 5). Since the two reactions can be broken into cycles having a common step of hydride addition, the different dependencies on X (reflected in part in a slope of 2.0 in Figure 5) would follow from differences pertaining to the strength of the Ir–CH₃ bond against the second Ir–H bonds. For some of the substituents, the larger dependence of ΔE_{MeH} on X can be attributed at least in part to steric effects. For example, when $X = O$ or S , the ΔE_{H_2} values are similar (-29.5

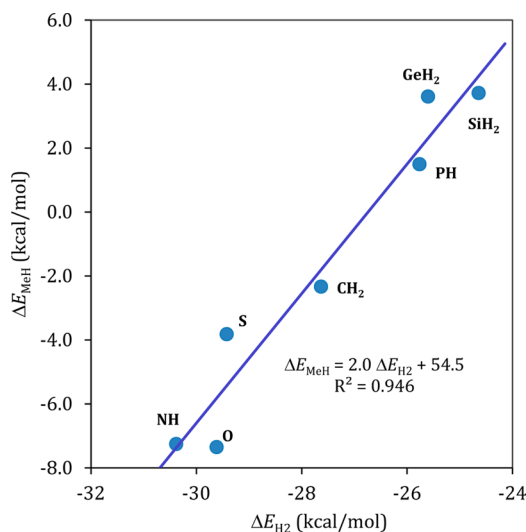


Figure 5. Comparison of the thermodynamics of H₂ and methane addition to 1-X leading to five-coordinate products in a Y-geometry.

kcal/mol). For methane addition, on the other hand, the ΔE_{CH_4} values for 1-O and 1-S are significantly different (-7.3 vs -3.8 kcal/mol). For both of these complexes the geometry is near C_{2v}. Table 1 shows that the methyl groups of the phosphines in 1-S are significantly closer to the empty coordination site than in 1-O: $r_1 = 5.6$ vs 4.7 Å. Thus, formation of an Ir–Me bond in 1-S is expected to have greater steric demands. Similar sterics based arguments can explain the greater difference in ΔE_{CH_4} in the reactions of 1-O and 1-CH₂ (-7.3 vs -2.3 kcal/mol) compared to the corresponding difference in ΔE_{H_2} (-29.6 vs -27.6 kcal/mol).

Finally, the computed transition state (TS) for C–H addition to 1-X has a geometry in which the Ir–H and Ir–Me bonds are only slightly longer than those of the distorted trigonal bipyramidal product, but the H–Ir–Me angle is significantly smaller (for example 44° in eq 3, which puts the hydride at 1.55 Å from the carbon of the methyl group). For all substituents, the imaginary frequency in the TS is near $600i$ cm⁻¹ and has coordinates corresponding to a bending mode of the H–Ir–Me angle dominated by motion of the hydride. Consistent with a product-like geometry, the energies of the TSs are only slightly higher (2.3 – 4.4 kcal/mol) than the energies of the products. A plot of the computed activation and reaction energies exhibits a linear correlation with a slope of 0.93 (Figure 6). Thus, the factors that influence the thermodynamics of the reaction, such as the electron and hydride affinities, bear direct implications to the kinetics.

CONCLUSIONS

We have used DFT methods to study the IE and EA trends of the pincer ligated Ir(^tBu⁴PXCXP) fragment (1-X), and to explore their utility in rationalizing the thermodynamic trends of the oxidative addition of H₂. The complexity of these seemingly simple transformations is greatly increased in the present system due to the accessibility of competing electronic states in the free radical cation and radical anion as well as the unsaturated five-coordinate dihydride product. Thus, the calculations afford different IE, EA, and reaction energy trends depending upon which state is considered. We attribute the variations in the different trends qualitatively to a combination of electronegativity (inductive) and π -MO (resonance) effects.

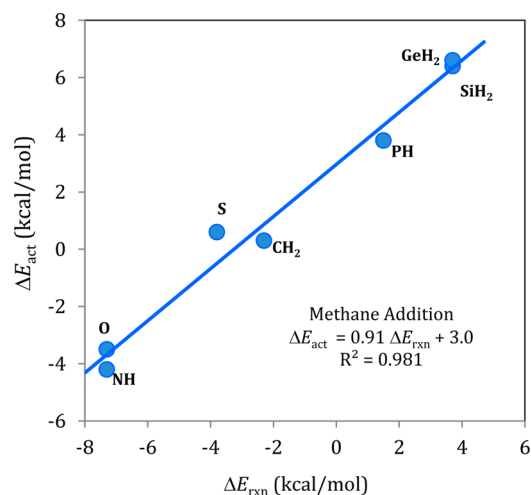


Figure 6. Plot of the activation energy of methane addition to 1-X against the reaction thermodynamics.

For example, when the thermodynamic Y-product is considered, H₂ addition to 1-O is found to be slightly more exothermic than addition to 1-CH₂ ($\Delta\Delta E_Y = 2.0$ kcal/mol). This is a counterintuitive result since the more electronegative oxygen linkers could be expected to reduce the electron density on the metal. We show that formation of the Y-product is associated with a change in the electronic state of 1-X such that a filled π -MO (d_{xz}) is emptied in the course of the reaction. Accordingly, a π -donor linker such as oxygen should favor an oxidative addition reaction leading to the Y-state. Consistently, the exothermicity order in the reaction of 1-O and 1-CH₂ is reversed for the higher energy T-dihydride product ($\Delta\Delta E_T = -5.5$ kcal/mol) where the occupancy of the π -MOs is not changed in the course of the reaction. Further analysis of the data using a hydride/proton addition cycle relates the greater exothermicity of H₂ addition to 1-O over 1-CH₂ ($\Delta\Delta E_Y = 2.0$ kcal/mol) to a favorable hydride affinity term ($\Delta\Delta HA_{dist} = 8.2$ kcal/mol) that is mitigated by a smaller proton affinity term ($\Delta\Delta PA_{dist} = -6.2$ kcal/mol). In this context, the π -effect that we propose to favor the reaction of 1-O would operate by yielding the smaller $\Delta\Delta PA_{dist}$ term. Additional calculations suggest this analysis can have relevance to the kinetics and thermodynamics of alkane C–H bond activation by 1-X. Such subtle effects exerted by varying the linkers in 1-X illustrate the challenges encountered in tuning this class of alkane dehydrogenation catalysts.

ASSOCIATED CONTENT

Supporting Information

Additional tables with electronic energies and Cartesian coordinates. This material is available free of charge via the Internet at <http://pubs.acs.org>.

AUTHOR INFORMATION

Corresponding Author

*E-mail: fh19@aub.edu.lb.

Present Address

^{||}Department of Chemistry, American University of the Middle East, Egaila, Kuwait.

Notes

The authors declare no competing financial interest.

ACKNOWLEDGMENTS

This work was supported by the Qatar National Research Fund, NPRP Grant 4-1517-1-245. HPC resources and services were provided by the IT Research Computing group in Texas A&M University at Qatar, supported by the Qatar Foundation for Education, Science and Community Development. Additional HPC resources were provided by the American University of Beirut.

REFERENCES

- (1) (a) van Koten, G.; Milstein, D. *Organometallic Pincer Chemistry (Topics in Organometallic Chemistry)*; Springer-Verlag: Heidelberg, 2013. (b) Morales-Morales, D.; Jensen, C. *The Chemistry of Pincer Compounds*; Elsevier: Amsterdam, 2007.
- (2) (a) van Koten, G. *J. Organomet. Chem.* **2013**, *730*, 156. (b) Schneider, S.; Meiners, J.; Askevold, B. *Eur. J. Inorg. Chem.* **2012**, *6*, 412. (c) Wang, Z.-X.; Ning, L. *Eur. J. Inorg. Chem.* **2012**, *6*, 901. (d) Bhattacharya, P.; Hairong, G. *Comments on Inorg. Chem.* **2011**, *32*, 88. (e) Ibrecht, M.; Lindner, M. M. *Dalton Trans.* **2011**, *40*, 8733. (f) Niu, J.-L.; Hao, X.-Q.; Gong, J.-F.; Song, M.-P. *Dalton Trans.* **2011**, *40*, 5135. (g) van der Vlugt, J. I. *Angew. Chem., Int. Ed.* **2010**, *49*, 252. (h) Moreno, I.; San Martin, R.; Herrero, M. T.; Dominguez, E. *Current Top. Catal.* **2009**, *8*, 91. (i) Limberg, C. *Angew. Chem., Int. Ed.* **2009**, *48*, 2270. (j) Pugh, D.; Danopoulos, A. A. *Angew. Chem., Int. Ed.* **2010**, *49*, 2007, 251, 610. (k) Peris, E.; Crabtree, R. H. *Angew. Chem., Int. Ed.* **2004**, *248*, 2239. (l) Singleton, J. T. *Tetrahedron* **2003**, *59*, 1837. (m) Rietveld, M. H. P.; Grove, D. M.; van Koten, G. *New J. Chem.* **1997**, *21*, 751. (n) Doherty, M. D.; Grills, D. C.; Huang, K.-W.; Muckerman, J. T.; Polyansky, D. E.; van Eldik, R.; Fujita, E. *Inorg. Chem.* **2013**, *52*, 4160.
- (3) Roddick, D. M. *Tuning of PCP Pincer Ligand Electronic and Steric Properties (Topics in Organometallic Chemistry)*; Springer-Verlag: Berlin, 2013.
- (4) Choi, J.; MacArthur, A. H. R.; Brookhart, M.; Goldman, A. S. *Chem. Rev.* **2011**, *111*, 1761.
- (5) Haibach, M. C.; Kundu, S.; Brookhart, M.; Goldman, A. S. *Acc. Chem. Res.* **2012**, *45*, 947.
- (6) Goldman, A. S.; Roy, A. H.; Huang, Z.; Ahuja, R.; Schinski, W.; Brookhart, M. *Science* **2006**, *312*, 257.
- (7) (a) Gupta, M.; Hagen, C.; Flesher, R. J.; Kaska, W. C.; Jensen, C. M. *Chem. Commun.* **1996**, 2083. (b) Gupta, M.; Kaska, W.; Jensen, C. M. *Chem. Commun.* **1997**, 461. (c) Liu, F.; Pak, E. B.; Singh, B.; Jensen, C. M.; Goldman, A. S. *J. Am. Chem. Soc.* **1999**, *121*, 4086.
- (8) Nawara-Hultsch, A. J.; Hackenberg, J. D.; Punji, B.; Supplee, C.; Emge, T. J.; Bailey, B. C.; Schrock, R. R.; Brookhart, M.; Goldman, A. S. *ACS Catal.* **2013**, *3*, 2505.
- (9) (a) Krogh-Jespersen, K.; Czerw, M.; Zhu, K.; Singh, B.; Kanzelberger, M.; Darji, N.; Achord, P. D.; Renkema, K. B.; Goldman, A. S. *J. Am. Chem. Soc.* **2002**, *124*, 10797. (b) Zhu, K.; Achord, P. D.; Zhang, X.; Krogh-Jespersen, K.; Goldman, A. S. *J. Am. Chem. Soc.* **2004**, *126*, 13044.
- (10) Renkema, K. B.; Kissin, Y. V.; Goldman, A. S. *J. Am. Chem. Soc.* **2003**, *125*, 7770.
- (11) Krogh-Jespersen, K.; Czerw, M.; Kanzelberger, M.; Goldman, A. S. *J. Chem. Inf. Comput. Sci.* **2001**, *41*, 56.
- (12) DuBois, D. L. *Inorg. Chem.* **2014**, *53*, 3935.
- (13) Kang, P.; Zhang, S.; Meyer, T. J.; Brookhart, M. *Angew. Chem., Int. Ed.* **2014**, *53*, 8709.
- (14) (a) Steffey, B. D.; Miedaner, A.; Maciejewski-Farmer, M. L.; Bernatis, P. R.; Herring, A. M.; Allured, V. S.; Carperos, V.; DuBois, D. L. *Organometallics* **1994**, *13*, 4844. (b) Doherty, M. D.; Konezny, S. J.; Batista, V. S.; Soloveichik, G. L. *J. Organomet. Chem.* **2014**, *762*, 94.
- (15) (a) Castonguay, A.; Beauchamp, A. L.; Zargarian, D. *Organometallics* **2008**, *27*, 5723. (b) Castonguay, A.; Spasyuk, D. M.; Madern, N.; Beauchamp, A. L.; Zargarian, D. *Organometallics* **2009**, *28*, 2134. (c) Gagliardo, M.; Havenith, R. W. A.; van Klink, G. P. M.; van Koten, G. *J. Organomet. Chem.* **2006**, *691*, 4411. (d) Gagliardo, M.; Dijkstra, H. P.; Coppo, P.; De Cola, L.; Lutz, M.; Spek, A. L.; van Klink, G. P. M.; van Koten, G. *Organometallics* **2004**, *23*, 5833.
- (16) Frisch, M. J.; et al. *Gaussian 09, Rev. A.02*; Gaussian, Inc.: Wallingford, CT, 2009.
- (17) Zhao, Y.; Truhlar, D. G. *Theor. Chem. Acc.* **2008**, *120*, 215.
- (18) (a) McLean, A. D.; Chandler, G. S. *J. Chem. Phys.* **1980**, *72*, 5639. (b) Raghavachari, K.; Binkley, J. S.; Seeger, R.; Pople, J. A. *J. Chem. Phys.* **1980**, *72*, 650. (c) Rassolov, V. A.; Ratner, M. A.; Pople, J. A.; Redfern, P. C.; Curtiss, L. A. *J. Comput. Chem.* **2001**, *22*, 976.
- (19) Hay, P. J.; Wadt, W. R. *J. Chem. Phys.* **1985**, *82*, 279.
- (20) Höllwarth, A.; Böhlert, A. W.; Bohme, M.; Dapprich, S.; Gobbi, A.; Höllwarth, A.; Jonas, V.; Köhler, K. F.; Stegmann, R.; Veldkamp, A.; Frenking, G. *Chem. Phys. Lett.* **1993**, *208*, 111.
- (21) See: <https://bse.pnl.gov/bse/portal>.
- (22) (a) Tomasi, J.; Persico, M. *Chem. Rev.* **1994**, *94*, 2027. (b) Cossi, M.; Scalmani, G.; Rega, N.; Barone, V. *J. Chem. Phys.* **2002**, *117*, 43.
- (23) Marenich, A. V.; Cramer, C. J.; Truhlar, D. G. *J. Phys. Chem. B* **2009**, *113*, 6378.
- (24) When two electronic states have similar energies, they can be subject to a pseudo-Jahn–Teller Effect that may require configuration interaction to be described adequately (see next reference for example). However, $[1-X^+]$ already has a low symmetry, and the two MOs defining the 2A and 2B states do not have common atomic coefficients, so there do not seem to be any obvious advantages to further distortion. Normal mode analysis confirms the given two states of the cation radical to be true minima on the PES.
- (25) (a) Vangberg, T.; Lie, R.; Ghosh, A. *J. Am. Chem. Soc.* **2002**, *124*, 8122. (b) Neeraj Kumar, N.; Kuta, J.; Galezowski, W.; Kozłowski, P. M. *Inorg. Chem.* **2013**, *52*, 1762.
- (26) (a) Rachidi, I. E.-I.; Eisenstein, O.; Jean, Y. *New J. Chem.* **1990**, *14*, 671. (b) Riehl, J. F.; Jean, Y.; Eisenstein, O.; Pelissier, M. *Organometallics* **1992**, *11*, 729.
- (27) Hasanayn, F.; Morris, R. H. *Inorg. Chem.* **2012**, *51*, 10808.
- (28) Bersuker, I. *Chem. Rev.* **2001**, *101*, 1067.
- (29) (a) Abu-Hasanayn, F.; Cheong, P.; Oliff, M. *Angew. Chem.* **2002**, *41*, 2120. (b) Hasanayn, F.; Markarian, M.-Z.; Al-Rifai, R. *Inorg. Chem.* **2004**, *43*, 3691.
- (30) Jensen, V.; Poli, R. *J. Phys. Chem. A* **2003**, *107*, 1424.
- (31) (a) Fryzuk, M. D.; MacNeil, P. A. *Organometallics* **1983**, *2*, 682. (b) Werner, H.; Hohn, A.; Dziallas, M. *Angew. Chem., Int. Ed.* **1986**, *25*, 1090. (c) Lunder, D. M.; Lobkovsky, E. B.; Streib, W. E.; Caulton, K. G. *J. Am. Chem. Soc.* **1991**, *113*, 1837. (d) Hauger, B. E.; Gusev, D.; Caulton, K. G. *J. Am. Chem. Soc.* **1994**, *116*, 208.
- (32) (a) Chin, B.; Lough, A. L.; Morris, R. H.; Schweitzer, C. T.; D'Agostino, C. *Inorg. Chem.* **1994**, *33*, 6278. (b) Wang, K.; Emge, T. G.; Goldman, A. S. *Organometallics* **1995**, *14*, 4929. (c) Goikhman, R.; Milstein, D. *Angew. Chem., Int. Ed.* **2001**, *40*, 1119.
- (33) (a) Abdur-Rashid, K.; Clapham, S. E.; Hadzovic, A.; Harvey, J. N.; Lough, A. J.; Morris, R. H. *J. Am. Chem. Soc.* **2002**, *124*, 15104. (b) Zimmer-De Iulius, M.; Morris, R. H. *J. Am. Chem. Soc.* **2009**, *131*, 11263.
- (34) Hadzovic, A.; Song, D.; MacLaughlin, C. M.; Morris, R. H. *Organometallics* **2007**, *26*, 5987.
- (35) (a) Noyori, R.; Hashiguchi, S. *Acc. Chem. Res.* **1997**, *30*, 97. (b) Noyori, R.; Ohkuma, T. *Angew. Chem., Int. Ed.* **2001**, *40*, 40. (c) Noyori, R. *Angew. Chem., Int. Ed.* **2002**, *41*, 2008.
- (36) For representative recent perspectives and reviews on electrocatalysis see: (a) DuBois, M. R.; Bullock, R. M. *Eur. J. Inorg. Chem.* **2011**, 1017. (b) Yang, J. Y.; Bullock, R. M.; DuBois, M. R.; DuBois, D. L. *MRS Bull.* **2011**, *36*, 39. (c) Bullock, R. M.; Apple, A. M.; Helm, M. L. *Chem. Commun.* **2014**, *50*, 3125. (d) Liu, T.; DuBois, M. R.; DuBois, D. L.; Bullock, R. M. *Energy Environ. Sci.* **2014**, *7*, 3630.
- (37) Mock, M. T.; Potter, R. G.; Camaioni, D. M.; Li, J.; Dougherty, W. G.; Kassel, W. S.; Twamley, B.; DuBois, D. L. *J. Am. Chem. Soc.* **2009**, *131*, 14454.
- (38) (a) Creutz, C.; Chou, M. H. *J. Am. Chem. Soc.* **2009**, *131*, 2794. (b) Creutz, C.; Chou, M. H.; Hou, H.; Muckerman, J. T. *Inorg. Chem.* **2010**, *49*, 9809. (c) Matsubara, Y.; Fujita, E.; Doherty, M. D.; Muckerman, J. T.; Creutz, C. *J. Am. Chem. Soc.* **2012**, *134*, 15743.

(d) Curtis, C. J.; Miedaner, A.; Raebiger, J. W.; DuBois, D. L. *Organometallics* **2004**, *23*, 511. (e) Zhu, Y.; Fan, Y.; Burgess, K. *J. Am. Chem. Soc.* **2010**, *132*, 6249.

(39) (a) Kovacs, G.; Papai, I. *Organometallics* **2006**, *25*, 820. (b) Qi, X.-J.; Fu, Y.; Liu, L.; Guo, Q.-X. *Organometallics* **2007**, *26*, 4197.

(40) (a) Solis, B. H.; Hammes-Schiffer, S. *Inorg. Chem.* **2014**, *53*, 6427. (b) Nimlos, M. R.; Chang, C. H.; Curtis, C. J.; Miedaner, A.; Pilath, H. M.; DuBois, D. L. *Organometallics* **2008**, *27*, 2715. (c) Chen, S.; Rousseau, R.; Raugei, S.; Dupuis, M.; Daniel, L.; DuBois, D. L.; Bullock, R. M. *Organometallics* **2011**, *30*, 6108. (d) Kang, S.-B.; Cho, Y. S.; Hwang, S. *Bull. Korean Chem. Soc.* **2009**, *30*, 2927. (e) James, T.; Muckerman, J. T.; Achord, P.; Creutz, C.; Polyansky, D. E.; Fujita, E. *Proc. Natl. Acad. Sci. U.S.A.* **2012**, *109*, 15657.

(41) Qi, X.-J.; Liu, L.; Fu, Y.; Guo, Q.-X. *Organometallics* **2006**, *25*, 5879.

(42) For a recent study including extensive references on the acidity of metal hydride and metal dihydrogen complexes see: Morris, R. H. *J. Am. Chem. Soc.* **2014**, *136*, 1948.

(43) We verified that the IE of the undistorted square planar $[1-X-H]^-$ anion is much larger than the distorted anion.

(44) Berning, D. E.; Miedaner, A.; Curtis, C. J.; Noll, B. C.; DuBois, M. R.; DuBois, D. L. *Organometallics* **2001**, *20*, 1832.

(45) Chen, S.; Ho, M.-H.; Bullock, R. M.; DuBois, D. L.; Dupuis, M.; Rousseau, R.; Raugei, S. *ACS Catal.* **2013**, *4*, 229.

(46) For the undistorted square planar $[1-X-H]^-$ complex, the lowest energy IE involves removal of an electron from the filled d_{xy} MO (p-type with b symmetry) rather than from the d_z^2 MO. The resulting 2B IEs continue to correlate satisfactorily with the proton affinities of the undistorted $[1-X-H]^-$.